

# The influence of roughness coefficient on hydrodynamic simulations: A case study at the Co Chien estuary, Mekong delta

NGUYEN Thi Kim Thao<sup>1,2,3\*</sup>, LE Van Tuan<sup>3</sup>

<sup>1</sup> Faculty of Physics and Engineering Physics, University of Science, Ho Chi Minh City, Vietnam

<sup>2</sup> Vietnam National University, Ho Chi Minh City, Vietnam

<sup>3</sup> Institute of Coastal and Offshore Engineering, Ho Chi Minh City, Vietnam, Vietnam

\* Corresponding email: kimthao.icoe@gmail.com

**Abstract:** Erosion in the Mekong Delta in general and the coastal area of Tra Vinh province in particular is still happening. One of the direct causes of erosion is due to hydrodynamic factors. Numerical modeling is important in studying and analyzing hydrodynamic regimes in coastal and estuarine areas. The reliability of simulation results heavily depends on the accurate determination of input parameters, among which the roughness coefficient is a crucial parameter. In coastal and estuarine areas, determining the value of the roughness coefficient is challenging due to the complex topography and hydrodynamic factors influenced by the combined effects of waves, currents, and tides. This study aims to assess the impact of the roughness coefficient (Manning's  $M$ - inverse of Manning's  $n$ ) on simulation results using the MIKE 21/3 Coupled Model FM at the Co Chien Estuary - one of the main branches of the Mekong River. The results show that as the Manning number ( $M$ ) increases, water level range and current speed rise, with  $M$  impact diminishing from the river mouth toward the sea.  $M$  notably affects spring tides more than neap tides, especially at tidal troughs and peak velocities. A Manning value of 40–50 provides reliable results. This study initially identifies a suitable range of Manning's  $M$  values for the study area, contributing to improving the reliability of numerical models.

**Keywords:** Numerical modeling; Manning roughness coefficient; Co Chien estuary; Mekong River.

## 1. Introduction

In recent years, erosion, landslides, saltwater intrusion, and many other issues related to water security in the Mekong Delta have become increasingly serious due to economic development in the upstream areas, climate change, and sea level rise [1], [2].

To address these challenges, initially, it is essential to understand hydrodynamic properties. Hydrodynamic research is an important and basic step before studying other issues such as erosion, pollution, saltwater intrusion, etc. There are many methods for studying hydrodynamics in rivers and seas. However, numerical simulation is still the most widely used method due to its speed, economy, and flexibility. Numerical simulation plays an important role in studying and analyzing hydrodynamic regimes in estuaries and coastal areas. These models allow simulation and prediction of complex phenomena such as waves, currents, tides, sediment transport, and diffusion of substances [3], [4].

Many scientific publications have used the MIKE 21/3 Coupled Model FM to study the hydrodynamic regime of estuaries and coastal areas. For example, a research has examined the hydrodynamic processes and coastal sediment transport near the coast of Bateau-cassé and Stamboul, Bay of Algiers [5]. Other study has used MIKE 21/3 model to study the dynamics along Purba Medinipur–Balasore coast, Bay of Bengal, India [6].

One of the largest deltas in the world, many hydrodynamic studies have been conducted in the Mekong Delta [7], [8]. A study analyzed the evolution and trends of erosion from 2016 to 2020 and identified the basic erosion mechanisms in the Mekong Delta region [9]. A recent study has shown that the average velocity at the Co Chien estuary is about 0.3 m/s, the farther away from the estuary the velocity decreases [10]. In work [11], tidal, current, and wave factors are identified as the main causes of erosion in this area.

The accuracy of the model depends on many factors. Suppose the input boundary conditions are assumed to be correct. In that case, the model will be calibrated with other hydraulic parameters, especially coefficients determined experimentally (there is no general formula for all applicable

conditions). In the hydrodynamic model, the roughness of the bottom layer has a great influence on the calculation results. Roughness is related to the problem of flow resistance, wave energy reduction, and the interaction of hydrodynamic factors with the bottom sediment. The roughness coefficient is declared through the Chezy or Manning number. The choice of the roughness coefficient is not easy because this quantity depends on many factors [12].

Determining the exact value of the roughness coefficient in coastal estuarine areas is a major challenge, due to the complexity of the terrain and various dynamic factors such as waves, currents, and tides. These factors often vary in time and space, making the selection of an appropriate roughness coefficient difficult [13], [14].

In 1889, Robert Manning presented the formula relating flow velocity and flow resistance coefficient in open channels [12]:

$$V = CR^{2/3}S^{1/2} \quad (1)$$

In which:

- + V (ft/s) is The average velocity of the flow in the channel;
- + C is a factor that represents flow resistance, influenced by the roughness of the channel surface;
- + R (ft) is the hydraulic radius, calculated as the cross-sectional area of flow divided by the wetted perimeter. It reflects the flow's effective depth in the channel;
- + S is the slope the channel, representing the gradient of the channel bed, often expressed as the change in elevation per unit length (dimensionless).

Formula (1) was later transformed into [12]:

$$V = \frac{1}{n}R^{2/3}S^{1/2} \quad (2)$$

In which: V (m/s) is the average velocity, R (m) is the hydraulic radius, and S is the slope, n is the roughness coefficient, also known as Manning's n.

Previous studies have shown that the value of the roughness coefficient depends on many factors such as terrain type, vegetation density, and hydrodynamic conditions of each area. In 1959, Chow provided a set of roughness coefficient values for different terrain types, from rivers with fine sand surfaces to areas with dense vegetation [12]. In addition, a study emphasized the role of seasonal variation and flow variability in determining roughness coefficients at different hydrological regions [15].

Some research articles focus on identifying factors that affect the Manning coefficient, as well as methods to determine the Manning coefficient more accurately. Empirical equations for predicting Manning's n are presented in the publication [16]. A recent study found that rainfall intensity, streamflow, surface roughness, and slope affect Manning's n. By using experimental methods, a study was conducted by varying rainfall intensity, flow rate, surface roughness, and slope. The results showed that Manning's n in the absence of rain increased as surface roughness increased and the inflow rate decreased [17].

Recently, many studies have been conducted to accurately determine the appropriate roughness coefficient for mathematical model input declaration. Some authors used the Dual-Annealing optimization method to automatically calibrate the model with non-uniform Manning coefficients [14]. Other research has explored how observation data from different (non-local) locations affect the estimation of Manning coefficients in tidal simulation models in large ocean areas such as the Bohai Sea, Yellow Sea, and East China Sea [18]. Manning's n roughness coefficient is also studied by a physical model with cases of changing bottom material, cases with and without hydraulic structures. The roughness coefficient with a weir was generally higher than that without one, indicating an increase in channel roughness. The roughness coefficient and discharge volume were mainly affected by channel slope, bed roughness, bed grain size, and bed shape [19].

In the MIKE model, the roughness coefficient is declared through Manning's number M (hereinafter referred to as the Manning number). This is the inverse value of Manning's number n. According to this definition, formula (2) can be rewritten as:

$$V = MR^{2/3}S^{1/2} \quad (3)$$

In which: M is the Manning number.

Several publications have addressed the application of this coefficient to some specific areas when simulating hydrodynamics. The Manning's n coefficient at a Nile River section, calibrated using an automatic method, ranges from 0.024 to 0.032, corresponding to Manning's M values ranging from 31 to 42 [14]. Manning's n coefficient was estimated to have an average value of 0.0246 (Manning's M is about 41) in shallow waters in a model over Yellow, Bohai and East China Seas [18]. In a hydrodynamic model to estimate the impact of intensive oyster farming using floating and fixed rafts on water exchange with application in Qinzhou Bay, China, the Manning number was reported to be 38 for the entire bay with depths ranging from 2 to -22 m [20]. Manning M values in the Mekong Delta region in some studies range from 20-45, depending on depth, vegetation, and bottom sediment characteristics [9].

Currently, there is no only formula that is widely applied to the Manning roughness coefficient in estuaries and coastal areas, due to the complexity of topographic, dynamic, and natural factors. Studies often calibrate the Manning coefficient based on the specific characteristics of each area and model conditions. In estuaries and coastal areas, the Manning roughness coefficient is greatly influenced by factors such as bottom topography, the combination of waves, currents, and tides, and biological factors (e.g., aquatic vegetation). Therefore, instead of using a fixed value, models often apply dynamic or segmented values of the Manning coefficient along different parts of the river and coastal area [14].

Hydrodynamic research on the Mekong Delta through numerical simulation is crucial in the context of climate change and sea level rise. The region is one of the largest deltas in the world but is highly vulnerable to sea level rise and changes in the Mekong River's flow. Numerical simulation enables the simulation of flow, sediment changes, and the impacts of flooding or salinity intrusion, thus helping to make more accurate predictions for the future. In-depth research on roughness coefficients is a key step to enhance the accuracy of mathematical model results. This not only supports the development of sustainable solutions in water resource management but also helps local communities and authorities better cope with the challenges posed by climate change.

Currently, authors have not yet established a consistent approach to the use of Manning's coefficient in simulation studies, leading to significant variations in results, even in regions with similar characteristics, such as estuaries, coastal zones, and offshore areas.

This study aims to assess the impact of roughness coefficients on hydrodynamic simulation results using the MIKE 21/3 Coupled model FM at the Co Chien estuary, one of the main tributaries of the Tien River. The research results will provide a suitable range of Manning's M values to improve the reliability of hydrodynamic models, thereby effectively supporting the study and protection of coastal estuaries.

## 2. Research methods and data

### 2.1. Research methods

Numerical simulation is the main method in this study. The MIKE 21/3 coupled model FM is used to simulate waves and currents in the calculated cases. In addition to the numerical simulation method, the data collection method is used to collect the necessary data for the study.

The collected data includes hydrological data and topographic data. Topographic data of the entire extended study area and neighboring areas are also collected to create a digital elevation grid as a rigid boundary for the model.

To conduct this study, the authors used a nested grid model including a general model and a detailed model. The general model includes all the main branches of the Mekong River. The inland border is limited by Can Tho, My Thuan, and Nha Be stations, extending to the sea about 63km from the shore. The detailed model is the area of the Co Chien and Cung Hau estuaries. These are the two estuaries of the Co Chien River. The Co Chien River is a main branch of the Tien River, the natural boundary of the two provinces of Ben Tre and Tra Vinh. The detailed study area has an area of 1,232 km<sup>2</sup> (see Fig. 1).



**Fig. 1.** Expanded (blue) and detailed (red) study areas of the model

## 2.2. Research data

To conduct this research, hard and soft boundaries need to be provided for the model. The hard boundary is the bottom topography of the entire study area. The soft boundary consists of hydrodynamic data (including flow and water levels) at the inland and sea boundaries.

The river boundary data is provided by the Southern Regional Hydro-Meteorological Center. These data are spatially fixed but vary over time, with a frequency of one data point per hour. The three sea boundaries consist of water level boundaries. The water level boundary is forecasted using the global tidal prediction model integrated into MIKE, which varies along the boundary and over time, with a frequency of one data point per hour (see Tab. 1).

The mathematical model also takes into account the effects of waves during the simulation period. The input wave fields are inherited from the results of the project in Tra Vinh province, code 21/HĐ-SKHCN. The wave field varies spatially and temporally across the entire computational domain, with a frequency of one dataset per hour.

After running the extended model, the input boundaries for the detailed model will be extracted. The extended model has been validated and is reliable enough to proceed with the next research steps.

The detailed model's input is derived from the extended model. The detailed model runs for January and July 2019, representing the Northeast and Southwest monsoon seasons, respectively. It will run for five hypothetical scenarios with M values of 20, 30, 40, 50, and 60. M is defined as a constant throughout the computational domain.

**Tab. 1.** Inputs of the extended model

No.	Model Boundary	Boundary Type	Time	Notes
1	Nha Be	Water Level	January 2019 (Northeast season) July 2019 (Southwest Season)	– Fixed in space, changing over time – Frequency 1 data per hour
2	My Thuan	Discharge		
3	Can Tho	Discharge		
4	3 coastal boundaries	Water Level Wave factors		– Changes along the boundary and over time – Frequency 1 hour 1 data

## 2.3. Evaluation of model error

To assess the reliability of the model, this study compares the calculated and observed results using NASH,  $R^2$ , and RMSE indices. These indices are commonly used to evaluate the accuracy and performance of hydrodynamic models.

NASH is an efficiency index used to evaluate the fit between simulation results and actual data. It compares the model's deviation to the mean of the observed data. The closer the NSE (Nash-Sutcliffe Efficiency) approaches 1, the more reliable the model is. An NSE below 0.36 is unsatisfactory, between 0.36 and 0.75 is satisfactory, and greater than 0.75 is considered very good [21], [22].

$R^2$  indicates the level of correlation between actual and simulated data.  $R^2$  ranges from 0 to 1.  $R^2 = 1$  indicates a perfect model, while  $R^2 = 0$  means the model does not explain the variation in the actual data [23], [24].

RMSE (Root Mean Square Error) measures the standard deviation of predictions from actual values. It indicates the level of difference between the predictions and observed data in the same units. The smaller the RMSE, the better, with the ideal value being  $RMSE = 0$ , which represents a model with no error. An RMSE below 0.5 is considered satisfactory [25], [22].

$$NSE = 1 - \frac{\sum_{i=1}^n (O_i - P_i)^2}{\sum_{i=1}^n (O_i - \bar{O})^2} \quad (4)$$

$$R^2 = \left( \frac{\sum (O_i - \bar{O})(P_i - \bar{P})}{\sqrt{\sum (O_i - \bar{O})^2 \cdot \sum (P_i - \bar{P})^2}} \right)^2 \quad (5)$$

$$RMSE = \sqrt{\frac{1}{n} \sum_{i=1}^n (P_i - O_i)^2} \quad (6)$$

Where:

- +  $O_i$  is the observed value;
- +  $P_i$  is the simulated value;
- +  $\bar{O}$  is the mean of the observed values.

The extended model is calibrated and verified with the above coefficients. The verification factors include water level, flow rate, and wave height. The verification results of the extended model meet the requirements and can be extracted for the detailed model to carry out the next research steps.

### 3. Results

#### 3.1. The impact of Manning's coefficient on hydrodynamic results

To analyze and clarify research results, three locations were extracted to compare the impact of Manning's coefficient on the calculation results, as shown in Fig. 2.

The selected positions represent the transition from riverine to marine environments, factoring in topography and hydrology. T1 is positioned in the main channel, where flow velocity is high due to strong tidal forces and river discharge. T2 is nearshore, in shallow waters affected by vegetation and bottom friction, and represents a primarily coastal area with minimal riverine influence, located away from the main channel. T3, the farthest offshore and deepest, lies in a deep-water area with minimal impact from nearshore factors (see detail at Tab. 2).

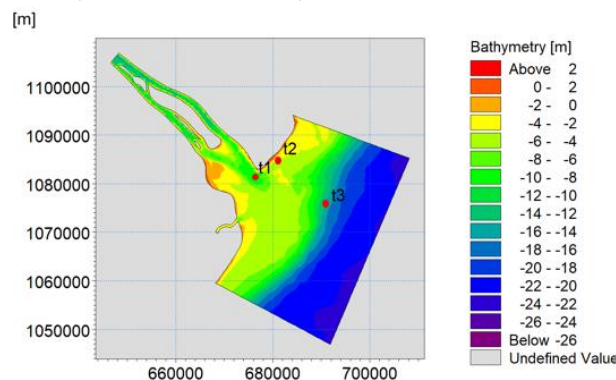


**Fig. 2.** Illustration of the comparison extraction position

**Tab. 2.** Comparison extraction positions

Extraction point	Coordinates (WGS 84 UTM zone 48N)		Bed Elevation	Notes
	X	Y		
	(m)	(m)	(m)	
T1	676139.47	1081266.01	-10.6	Location in the main channel of the river mouth
T2	681239.73	1085164.37	-4.0	Nearshore location
T3	691183.57	1075614.81	-14.5	Offshore location

3.1.1.1. January - Northeast season

3.1.1.1.1. Water level

As the Manning number (Manning) value increases, the water level range also tends to rise, reflecting a positive correlation between this value and the water level range. From T1 to T3, the impact of Manning gradually decreases, showing that areas strongly influenced by river flow, such as at T1, respond more distinctly to changes in Manning. At T3 (offshore area), the impact of Manning on the water level is extremely small, almost unchanged. Notably, as the Manning value continues to rise, the degree of influence on the increase in water level range gradually diminishes, demonstrating a decreasing effect of the Manning number in these areas (see Tab. 3).

**Tab. 3.** Water level characteristics in the scenarios, January

No.	M value	Point	Min (m)	Max (m)	Mean (m)	Standard Dev (m)	Range Water level range (m)	Water level range difference compared to the previous M value.	
								(m)	%
1	20	T1	-1.42	1.59	0.13	0.75	3.01		
2	30	T1	-1.79	1.64	0.08	0.84	3.43	0.42	14.0%
3	40	T1	-2.06	1.69	0.05	0.90	3.76	0.33	9.6%
4	50	T1	-2.26	1.73	0.03	0.94	3.99	0.23	6.1%
5	60	T1	-2.41	1.76	0.02	0.97	4.16	0.17	4.3%
1	20	T2	-2.13	1.63	0.04	0.88	3.76		
2	30	T2	-2.36	1.65	0.02	0.93	4.01	0.25	6.6%
3	40	T2	-2.48	1.67	0.01	0.95	4.15	0.14	3.5%
4	50	T2	-2.57	1.69	0.01	0.97	4.26	0.11	2.7%
5	60	T2	-2.64	1.70	0.00	0.97	4.34	0.08	1.9%
1	20	T3	-2.66	1.67	0.00	0.97	4.33		
2	30	T3	-2.67	1.68	0.00	0.98	4.35	0.02	0.5%
3	40	T3	-2.67	1.69	0.00	0.98	4.36	0.01	0.2%
4	50	T3	-2.68	1.70	0.00	0.98	4.38	0.02	0.5%
5	60	T3	-2.68	1.70	0.00	0.98	4.38	0.00	0.0%

Extract the water level results at three points under different Manning scenarios during the neap tide period from January 13-17, 2019, and the spring tide period from January 22-25, 2019. The results are shown in Fig. 3. It can be observed that during the spring tide period, the influence of the Manning number is greater than during the neap tide period at T1 and T2 points, especially at tidal troughs. This indicated an asymmetry in the influence of Manning on tidal phases.

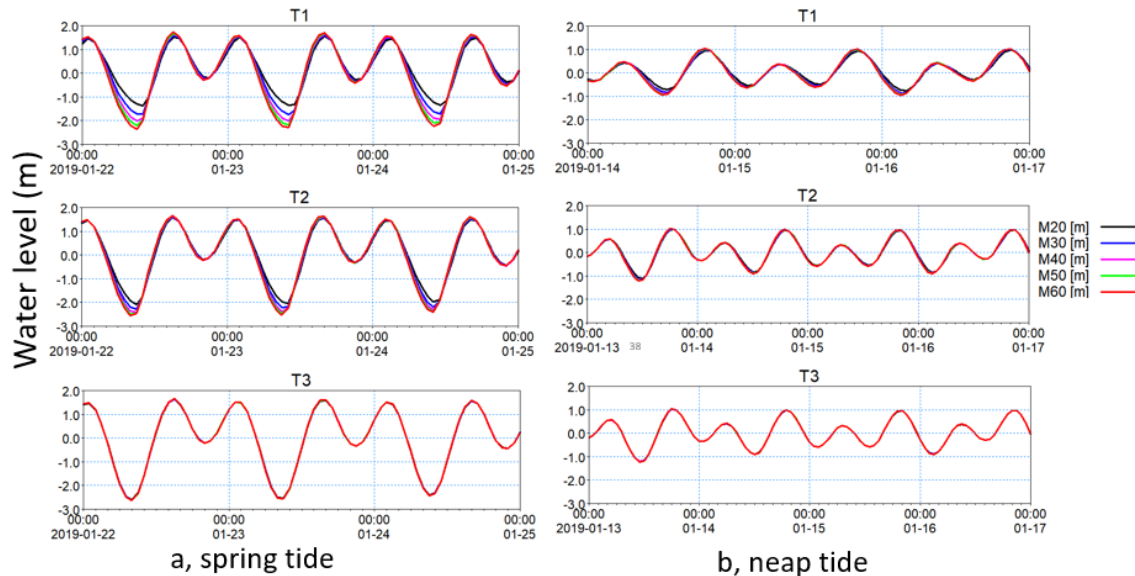


**Fig. 3.** Water levels at three points were extracted from the scenarios in January

3.1.1.2. Current speed

Current speed tends to increase as the Manning value rises; however, similar to water levels, the velocity sensitivity to changes in Manning gradually decreases as the Manning value increases. The deep channel position at the river mouth (T1) shows the highest sensitivity to changes in Manning, and this trend decreases from the river toward the sea. When the Manning value reaches 50 and 60, the difference in velocity between these two cases becomes very small, ranging from 1.9% to 3.4%, indicating a decrease in the effect of Manning on Current speed at these locations (see Tab. 4).

The further away from the river mouth, the smaller this difference becomes. Extract the velocity results at three points under different Manning scenarios during the neap tide and the spring tide. During spring tides, the impact is greater than during neap tides, especially at points where the velocity reaches its maximum. The estuary areas (T1) are most affected by this parameter, while offshore locations (T3) show minimal influence (Tab. 4, Fig. 4).

**Tab. 4.** Current speed characteristics in the scenarios in January

TT	M value	Point	Min	Max	Mean	Standard Dev	The mean difference compared to the previous M value	
			(m/s)	(m/s)	(m/s)	(m/s)	(m/s)	%
1	20	T1	0.012	0.702	0.299	0.181		
2	30	T1	0.015	0.904	0.375	0.225	0.076	25.4%
3	40	T1	0.019	1.045	0.411	0.257	0.036	9.6%
4	50	T1	0.009	1.156	0.427	0.280	0.016	3.9%
5	60	T1	0.008	1.244	0.435	0.296	0.008	1.9%
1	20	T2	0.007	0.365	0.158	0.086		
2	30	T2	0.006	0.461	0.194	0.108	0.036	22.8%

3	40	T2	0.007	0.523	0.212	0.123	0.018	9.3%
4	50	T2	0.006	0.561	0.221	0.131	0.009	4.2%
5	60	T2	0.016	0.578	0.227	0.135	0.006	2.7%
1	20	T3	0.006	0.317	0.134	0.066		
2	30	T3	0.004	0.371	0.156	0.078	0.022	16.4%
3	40	T3	0.007	0.406	0.168	0.087	0.012	7.7%
4	50	T3	0.003	0.432	0.176	0.095	0.008	4.8%
5	60	T3	0.003	0.453	0.182	0.102	0.006	3.4%

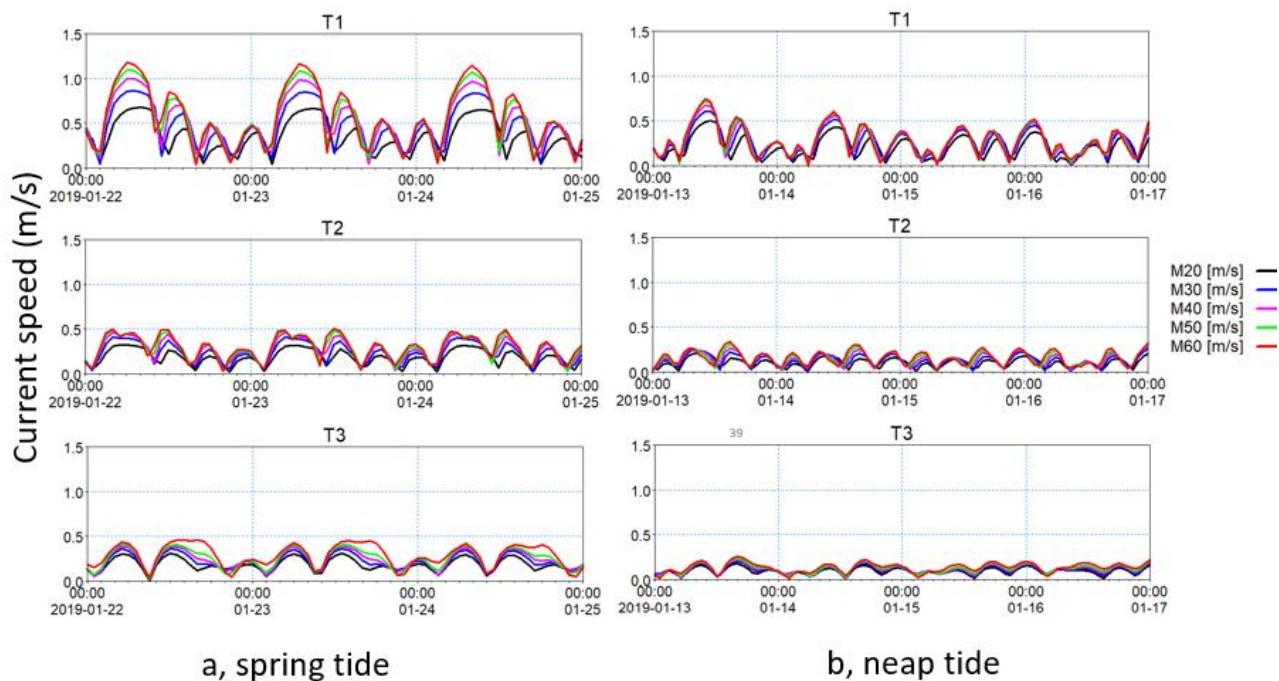


**Fig. 4.** Current speed at three points was extracted from the scenarios in January

### 3.1.2. July - Southwest Season

#### 3.1.2.1. Water level

Tab. 5 shows the water level characteristics at three points T1, T2, and T3 under different M scenarios. T1 and T2 exhibit a clear change in water level amplitude as the Manning value increases, particularly in the range from M equal to 20 to 30. However, the rate of increase in amplitude gradually decreases at higher Manning values. T3 shows more stability in amplitude, with very little change when Manning varies, indicating that this area is less sensitive to the Manning number.

Extract the water level results at three points under different M scenarios during the spring tide period from July 16-19, 2019, and the neap tide period from January 24-27, 2019. The results are shown in Fig. 5. Similar to the Northeastern Winter case, it can be observed that during the spring tide period, the influence of the Manning number is greater than during the neap tide period at T1 and T2 points, especially at tidal troughs.

**Tab. 5.** Water level characteristics in the scenarios in July

No.	M value	Point	Min (m)	Max (m)	Mean (m)	Standard Dev (m)	Water level range (m)	Water level range difference compared to the previous M value.	
								Value (m)	%
1	20	T1	-1.45	1.52	0.13	0.75	2.97		
2	30	T1	-1.83	1.59	0.08	0.84	3.42	0.45	15.2%
3	40	T1	-2.09	1.63	0.05	0.90	3.72	0.30	8.8%
4	50	T1	-2.26	1.65	0.03	0.94	3.90	0.18	4.8%
5	60	T1	-2.36	1.64	0.02	0.96	4.00	0.10	2.6%
1	20	T2	-2.09	1.54	0.04	0.87	3.63		
2	30	T2	-2.31	1.57	0.02	0.92	3.88	0.25	6.9%
3	40	T2	-2.46	1.59	0.01	0.94	4.05	0.17	4.4%
4	50	T2	-2.55	1.59	0.01	0.96	4.14	0.09	2.2%
5	60	T2	-2.61	1.60	0.00	0.96	4.21	0.07	1.7%
1	20	T3	-2.59	1.57	0.00	0.97	4.15		
2	30	T3	-2.60	1.58	0.00	0.97	4.18	0.03	0.7%
3	40	T3	-2.61	1.58	0.00	0.98	4.19	0.01	0.2%
4	50	T3	-2.61	1.59	0.00	0.98	4.21	0.02	0.5%
5	60	T3	-2.61	1.60	0.00	0.98	4.21	0.00	0.0%

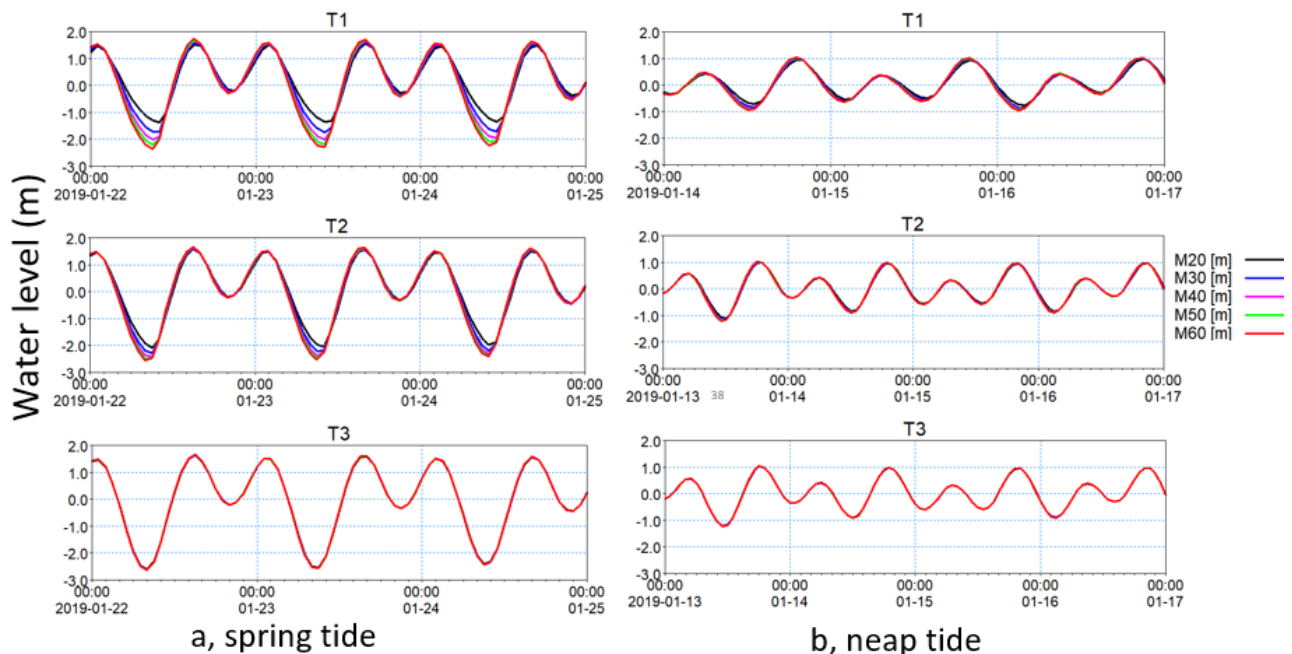


**Fig. 5.** Water levels at three points were extracted from the scenarios in July

3.1.2.2. Current speed

At all extraction points T1, T2, and T3, current speed fluctuates under the influence of the tide, with peaks and troughs corresponding to the rise and fall of the tide. As the water level amplitude increases, the current speed also increases. The greater the current speed, the greater the influence of the Manning

number (see Tab. 6). During the spring tide period, the impact of Manning is greater compared to the neap tide period. Notably, when the tide recedes, with high current speed and low water levels, the effect of bottom friction on the simulation results becomes more pronounced (Fig. 6).

**Tab. 6.** Current speed characteristics in the scenarios in July

TT	M value	Point	Min (m/s)	Max (m/s)	Mean (m/s)	Standard Dev (m/s)	The mean difference compared to the previous M value.	
							Value (m/s)	%
1	20	T1	0.004	0.656	0.267	0.174		
2	30	T1	0.004	0.833	0.333	0.219	0.066	24.7%
3	40	T1	0.012	0.969	0.365	0.251	0.032	9.6%
4	50	T1	0.013	1.074	0.381	0.275	0.016	4.4%
5	60	T1	0.006	1.153	0.389	0.293	0.008	2.1%
1	20	T2	0.010	0.317	0.142	0.080		
2	30	T2	0.010	0.400	0.174	0.099	0.032	22.5%
3	40	T2	0.012	0.448	0.192	0.111	0.018	10.3%
4	50	T2	0.015	0.478	0.200	0.119	0.008	4.2%
5	60	T2	0.016	0.500	0.203	0.124	0.003	1.5%
1	20	T3	0.005	0.304	0.138	0.065		
2	30	T3	0.003	0.358	0.161	0.078	0.023	16.7%
3	40	T3	0.004	0.394	0.172	0.087	0.011	6.8%
4	50	T3	0.010	0.424	0.180	0.095	0.008	4.7%
5	60	T3	0.006	0.447	0.193	0.106	0.013	7.2%

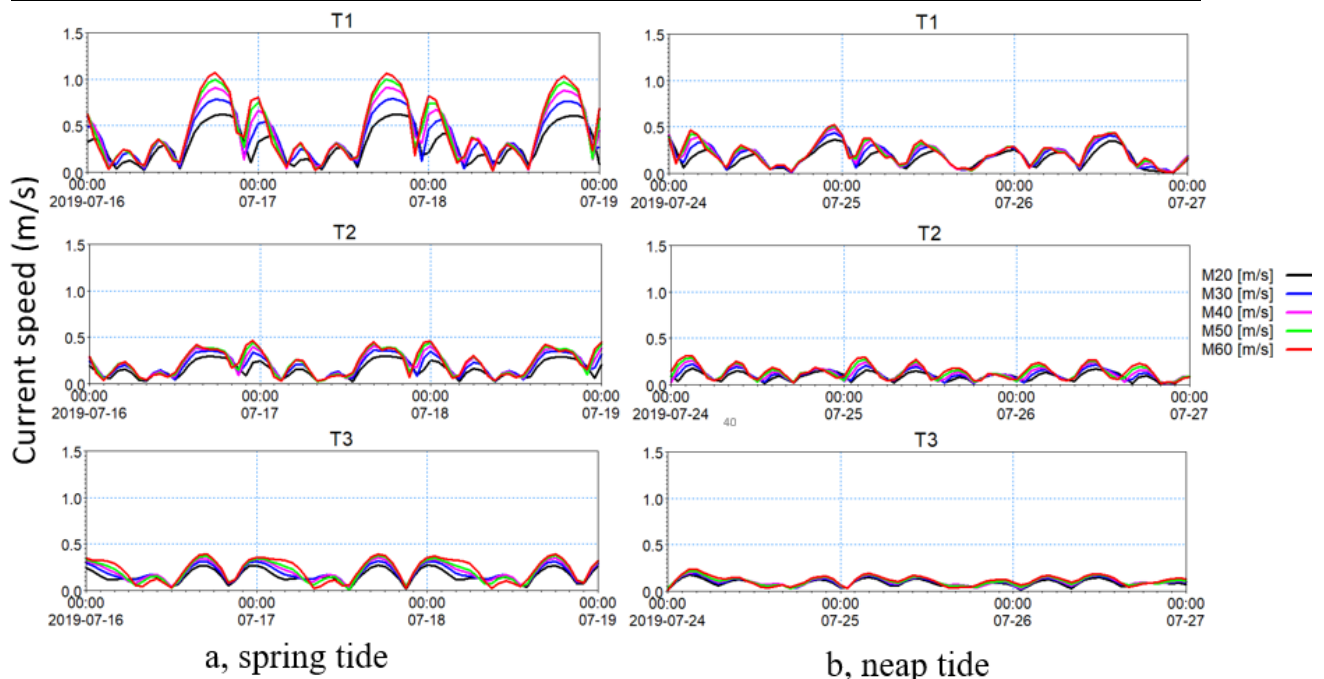


**Fig. 6.** Current speed at three points was extracted from the scenarios in July

### 3.2. Comparison with actual measured data

Extract and compare the agreement between the actual measured data at Ben Trai station (BT) and the simulation cases with different Manning's coefficients (see the illustration of Ben Trai station's location in Fig. 7). Fig. 8 and Fig. 9 illustrate the measured and simulated water levels at Ben Trai station in January, during the spring tide and neap tide periods, respectively. Fig. 10 and Fig. 11 illustrate the measured and simulated water levels at Ben Trai station in July, during the spring tide and neap tide periods, respectively.

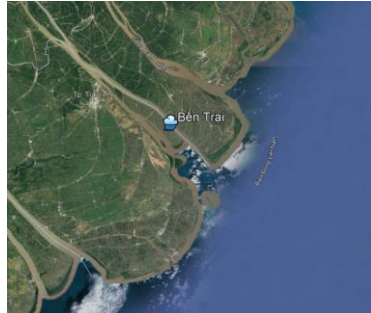


**Fig. 7.** Illustration of the location of Ben Trai stations

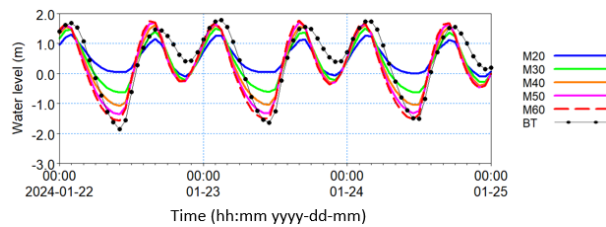


**Fig. 8.** Comparison of measured and simulated water levels at Ben Trai station in January, spring tide

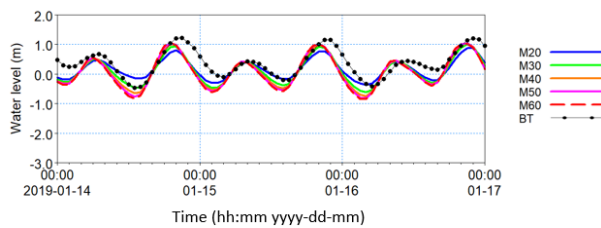


**Fig. 9.** Comparison of measured and simulated water levels at Ben Trai station in January, neap tide

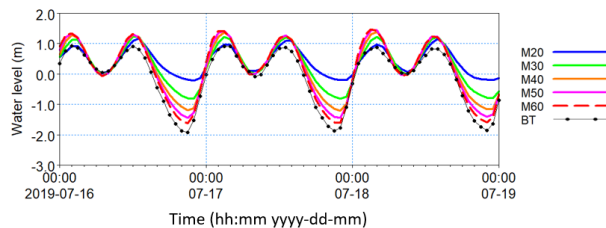


**Fig. 10.** Comparison of measured and simulated water levels at Ben Trai station in July, spring tide

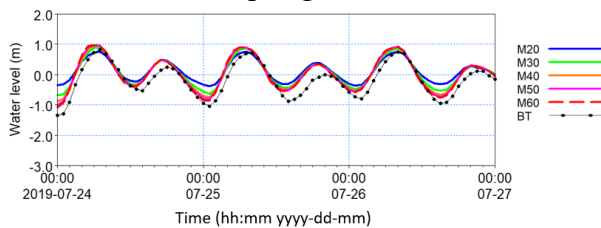


**Fig. 11.** Comparison of measured and simulated water levels at Ben Trai station in July, neap tide

Fig. 12 shows the correlation between the actual measured water levels and the simulation cases with different M values for January and July. M=40 performs best in January, while M=50 and M=60 perform best in July. M=20 consistently shows the lowest correlation in both months. To further assess model accuracy for each M value, the study calculated additional performance indicators, including NSE and RMSE, as shown in Tab. 7. In January, all NSE values exceed the threshold (>0.36), with M values of 30 and 40 achieving the highest NSE (0.71). RMSE values for M=20 and M=60 do not meet the requirement (>0.5), while M=30 and M=40 show the best (lowest) RMSE values. In July, M=20 does not meet the NSE requirement. The highest NSE values are found in M=60 and M=50, at 0.85 and 0.84, respectively. Averaging across both January and July, M=40 and M=50 achieve the highest NSE and R<sup>2</sup> values, and also have the lowest average RMSE values, closely at 0.39 and 0.40 (Tab 7).

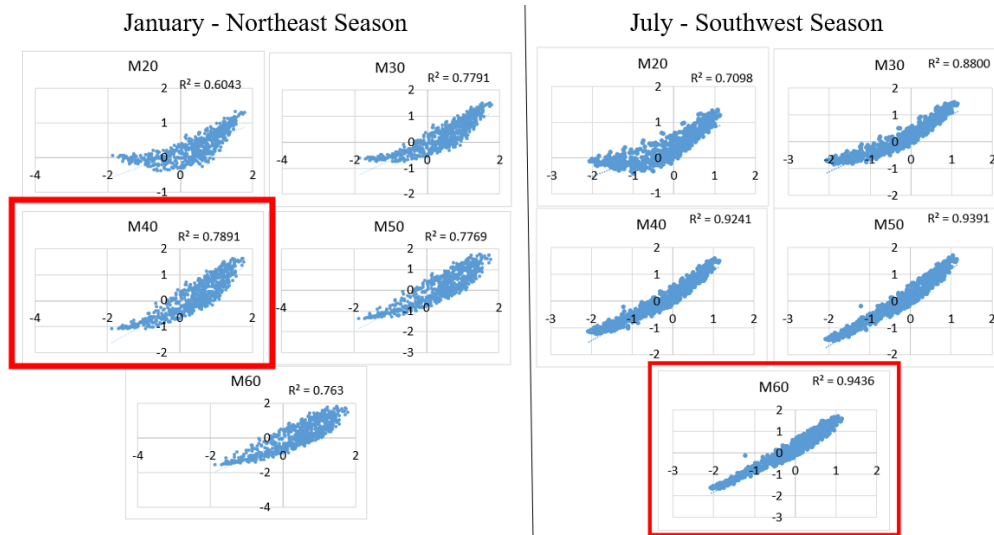


**Fig. 12.** Correlation between measured and simulated water levels at Ben Trai station

**Tab. 7.** Assessment of the agreement between calculations and measurement at Ben Trai station

TT	M	Northeast Monsoon - January			Southwest Monsoon - July			The average of the two months		
		NSE	R <sup>2</sup>	RMSE	NSE	R <sup>2</sup>	RMSE	NSE	R <sup>2</sup>	RMSE
1	M20	0.52	0.60	0.55	0.30	0.71	0.67	0.41	0.66	0.61
2	M30	0.71	0.78	0.43	0.66	0.88	0.46	0.69	0.83	0.45
3	M40	0.71	0.79	0.43	0.79	0.92	0.37	0.75	0.86	0.40
4	M50	0.66	0.78	0.46	0.84	0.94	0.32	0.75	0.86	0.39
5	M60	0.61	0.76	0.50	0.85	0.94	0.31	0.73	0.85	0.40

#### 4. Discussions

At the extraction points, the water level displays semi-diurnal tide characteristics, with two high and two low tides per day. The peaks and troughs are uneven, especially during spring tides, leading to four daily velocity peaks that align with rising and falling tides. Greater water level range correspond to higher flow velocities, consistent with the region’s tidal dynamics [25].

Increasing the Manning number raises the water level and current speed, as it inversely affects the friction coefficient, reducing flow resistance. Near the river mouth (T1), changes in Manning number significantly impact flow, particularly during low tides when reduced water depth amplifies frictional effects, allowing faster-receding tides and deeper troughs. Conversely, the offshore area (T3) is largely unaffected by Manning number changes. In offshore, the dominant dynamic factors such as tidal and wave forces are often significantly larger in scale than the effects of bottom friction. Besides, the terrain at sea is usually flat and does not change rapidly. Therefore, the influence of roughness changes on the offshore hydrodynamic system is often minimized and less sensitive.

Comparing models, A Manning number of 20 yields the least accurate results in both months.

Manning numbers between 40 and 50 best simulate hydrodynamics, with better accuracy in July (Southwest Monsoon) than in January (Northeast Monsoon). Comparison with the domain-variable values selected in the study [9] is quite suitable.

## 5. Conclusion

As the Manning number (M) increases, both water level range and current speed rise, with M impact diminishing from the river mouth toward the sea. At T3 (offshore area), the impact of Manning on the water level is extremely small, almost unchanged. M notably affects spring tides more than neap tides, especially at tidal troughs and peak velocities. A Manning value of 40–50 provides reliable results and is suitable for simulations across seasons.

**The vastness of the Mekong Delta presents challenges in obtaining uniform terrain data. Bottom topography data were collected from diverse sources at varying times and densities, making it difficult to maintain complete uniformity or the latest data in certain areas.**

This study only compared short-term water level data for January and July, without including current speed or discharge data. Future research will deepen this analysis by incorporating these metrics once additional reliable data is available, allowing for a more precise determination of the ideal Manning values for the area.

## Acknowledgments

This study was conducted with the support of the provincial-level project “Review and assessment of the safety of the embankment, dyke, and sluice gate systems in the estuarine and coastal areas due to erosion and storm surges, and proposal of solutions to ensure resilience during the 2025-2035 period in Tra Vinh province” code 21/HĐ-SKHCN.

## Literature – References

1. Orieschnig, C., Venot, J.-P., Massuel, S., Eang, K.E., Chhuon, K., Lun, S. et al. (2022) A Multi-Method Approach to Flood Mapping: Reconstructing Inundation Changes in the Cambodian Upper Mekong Delta. *Journal of Hydrology*, 610, 127902. <https://doi.org/10.1016/j.jhydrol.2022.127902>
2. Hoang, L.P., Lauri, H., Kumm, M., Koponen, J., van Vliet, M.T.H., Supit, I. et al. (2016) Mekong River flow and hydrological extremes under climate change. *Hydrology and Earth System Sciences, Copernicus GmbH*, 20, 3027–41. <https://doi.org/10.5194/hess-20-3027-2016>
3. Xiao, H., Zhang, Z., Tang, Y., Li, H. and Tang, Q. (2024) Numerical modeling for determination of the dominant factor inducing saltwater intrusion into shallow aquifer in the Mekong River Estuary within the Mekong Delta, Vietnam. *Sustainable Horizons*, 12, 100111. <https://doi.org/10.1016/j.horiz.2024.100111>
4. Lai, Y.G. (2024) An Integrated Current–Wave–Sediment Model for Coastal and Estuary Simulation. *Water, Multidisciplinary Digital Publishing Institute*, 16, 415. <https://doi.org/10.3390/w16030415>
5. Dahmani, A. el alim, Mezouar, K., Salem Cherif, Y. and Sallaye, M. (2021) Coastal processes and nearshore hydrodynamics under high contrast wave exposure, Bateau-cassé and Stamboul coasts, Algiers Bay. *Estuarine, Coastal and Shelf Science*, 250, 107169. <https://doi.org/10.1016/j.ecss.2021.107169>
6. Mandal, S. and Chaudhuri, S. (2023) Identification of littoral cell and its impact on shoreline dynamics along the Purba Medinipur–Balasore coastal stretch, Bay of Bengal, India: A numerical modelling and geospatial study. *Regional Studies in Marine Science*, 57, 102740. <https://doi.org/10.1016/j.rsma.2022.102740>
7. Morovati, K., Tian, F., Pokhrel, Y., Someth, P., Shi, L., Zhang, K. et al. (2024) Fishery and agriculture amidst human activities and climate change in the Mekong River: A review of gaps in data and effective approaches towards sustainable development. *Journal of Hydrology*, 644, 132043. <https://doi.org/10.1016/j.jhydrol.2024.132043>
8. Yun, X., Song, J., Wang, J. and Bao, H. (2024) Modelling to assess the suitability of hydrological-hydrodynamic model under the hydropower development impact in the Lancang-Mekong river basin. *Journal of Hydrology*, 637, 131393. <https://doi.org/10.1016/j.jhydrol.2024.131393>
9. Pham, H.T.H. and Bui, L.T. (2023) Mechanism of erosion zone formation based on hydrodynamic factor analysis in the Mekong Delta coast, Vietnam. *Environmental Technology & Innovation*, 30, 103094. <https://doi.org/10.1016/j.eti.2023.103094>

10. Vu, M.T., Luu, C., Bui, D.Q., Vu, Q.H. and Pham, M.Q. (2024) Simulation of hydrodynamic changes and salinity intrusion in the lower Vietnamese Mekong Delta under climate change-induced sea level rise and upstream river discharge. *Regional Studies in Marine Science*, 78, 103749. <https://doi.org/10.1016/j.rsma.2024.103749>
11. Le, X.H., Kim, Y., Van Binh, D., Jung, S., Hai Nguyen, D. and Lee, G. (2024) Improving rainfall-runoff modeling in the Mekong river basin using bias-corrected satellite precipitation products by convolutional neural networks. *Journal of Hydrology*, 630, 130762. <https://doi.org/10.1016/j.jhydrol.2024.130762>
12. Chow, V. te. (1959) *Open-Channel Hydraulics*. MC Graw Hill Seattle, WA.
13. Silva-Cancino, N., Salazar, F., Bladé, E. and Sanz-Ramos, M. (2024) Influence of breach parameter models on hazard classification of off-stream reservoirs. *Water Science and Engineering*, <https://doi.org/10.1016/j.wse.2024.05.001>
14. Abouelsaad, O., Hassan, A., Omar, M. and Hinkelmann, R. (2024) Identifying manning roughness coefficient using automatic calibration method and simulation of pollution incidents in the Nile River, Egypt. *Journal of Hydrology: Regional Studies*, 55, 101908. <https://doi.org/10.1016/j.ejrh.2024.101908>
15. Arcement, G.J. and Schneider, V.R. (1989) Guide for selecting Manning's roughness coefficients for natural channels and flood plains [Internet]. US Geological Survey, United States.
16. Lang, S., Ladson, T. and Anderson, B. (2004) A review of empirical equations for estimating stream roughness and their application to four streams in Victoria. *Australasian Journal of Water Resources*, Taylor & Francis. 8, 69–82.
17. Shen, E., Liu, G., Dan, C., Chen, X., Ye, S., Li, R. et al. (2023) Estimating Manning's coefficient for sheet n during rainstorms. *CATENA*, 226, 107093. <https://doi.org/10.1016/j.catena.2023.107093>
18. Wei, Z., Zhang, J., Wang, D., Gao, Y. and Cheng, J. (2024) The effects of non-local observations on the adjoint estimation of local model parameters: An example of Manning's coefficient in a tidal model over the Bohai, Yellow, and East China Seas. *Journal of Hydrology*, 131437. <https://doi.org/10.1016/j.jhydrol.2024.131437>
19. Amsie, A.B., Ayalew, A.T., Mada, Z.M. and Finsa, M.M. (2024) Acclimatize experimental approach to adjudicate hydraulic coefficients under different bed material configurations and slopes with and without weir. *Heliyon*, 10, e32162. <https://doi.org/10.1016/j.heliyon.2024.e32162>
20. Huang, Y., Li, Z., Sun, C., Feng, Z., Li, J., Wei, D. et al. (2023) Using the roughness height and manning number in hydrodynamic model to estimate the impact of intensive oyster aquaculture by floating & fixed rafts on water exchange with an application in Qinzhou Bay, China. *Ecological Modelling*, 476, 110230. <https://doi.org/10.1016/j.ecolmodel.2022.110230>
21. Nash, J.E. and Sutcliffe, J.V. (1970) River flow forecasting through conceptual models part I — A discussion of principles. *Journal of Hydrology*, 10, 282–90. [https://doi.org/10.1016/0022-1694\(70\)90255-6](https://doi.org/10.1016/0022-1694(70)90255-6)
22. Moriasi, D.N., Arnold, J.G., Van Liew, M.W., Bingner, R.L., Harmel, R.D. and Veith, T.L. (2007) Model evaluation guidelines for systematic quantification of accuracy in watershed simulations. *Transactions of the ASABE, American society of agricultural and biological engineers*. 50, 885–900.
23. Mohd Salleh, S.H., Wan Mohtar, W.H.M., Abdul Maulud, K.N., Haron, N.F., Abd Rashid, N. and Awang, N.A. (2025) Performance evaluation of high discharge estuarine hydrodynamic model. *Ain Shams Engineering Journal*, 16, 103322. <https://doi.org/10.1016/j.asej.2025.103322>
24. Pranowo, W. and Ramadhani, A.R. (2025) Error-based correlation coefficient: An alternative to combine error and coefficient of correlation and its application in geophysical data. *Journal of Computational Science*, 88, 102611. <https://doi.org/10.1016/j.jocs.2025.102611>
25. Shen, Y., Liu, D., Jiang, L., Yin, J., Nielsen, K., Bauer-Gottwein, P. et al. (2020) On the Contribution of Satellite Altimetry-Derived Water Surface Elevation to Hydrodynamic Model Calibration in the Han River. *Remote Sensing, Multidisciplinary Digital Publishing Institute*. 12, 4087. <https://doi.org/10.3390/rs12244087>
26. Nguyen Xuan, L., Nguyen Le, T., Tran Anh, Q. and Trinh Tuan, L. (2024) Estimation of tidal energy potential in the Vietnam East Sea: A comprehensive analysis using semi-empirical tide models. *Regional Studies in Marine Science*, 80, 103859. <https://doi.org/10.1016/j.rsma.2024.103859>